Iranian Journal of Geophysics, Vol 20 No 6, 2027, Page 17 – 35 (Research Article)
DOI: 10.30499/ijg.2025.510947.1682

Mapping the shallow-to-deep subsurface structural elements to determine the thermal region and hydrocarbon potential of Gongola basin, NE Nigeria

Taiwo Adewumi[1*], Oladiran Johnson Abimbola[2], Abubarka Umar Madaki[3], Babatope Ebenezer Faweya[4], Kazeem Adeyinka Salako[5], Nordiana Mohd Muztaza[6] and Fidelis Iorzua Kwaghhua[7]

[1] *Assistant Professor, Department of Physics, Faculty of Science, Federal University of Lafia, Nigeria*
[2] *Professor, Department of Physics, Faculty of Science, Federal University of Lafia, Nigeria*
[3] *M.Sc., Department of Physics, Faculty of Science, Federal University of Lafia, Nigeria*
[4] *Professor, Department of Physics, Faculty of Science, Ekiti State University, Nigeria*
[5] *Professor, Department of Geophysics, School of Physical Science, Federal University of Technology Minna, Nigeria*
[6] *School of Physics, University Sains Malaysia (USM), Malaysia*
[7] *Ph.D. Student,Professor, Department of Geophysics, School of Physical Science, Federal University of Technology Minna, Nigeria*

(Received: 09 March 2025, Accepted: 25 August 2025)

Abstract

The study aims to provide new insights into the subsurface crustal and thermal structures of the Gongola Basin, NE Nigeria, using airborne magnetic and gamma-ray spectrometric datasets for hydrocarbon prospecting. The total magnetic field, reduced to the magnetic equator (TMI-RTE), underwent various enhancement techniques and depth estimation methods, including vertical derivative (VD), Rose diagram (RD), source parameter imaging (SPI), and 2D magnetic depth modelling to distinctly map the subsurface geological structural elements, basement architecture, and the depth to the top of the magnetic basement. Conversely, the radiogenic heat production (RHP) and regions favourable for hydrocarbon maturation and accumulation were determined via thorium normalisation techniques (TNT) from the concentration of radioactive elements (K, eTh, and eU). The FVD, SVD, and RD indicate that the dominant structures within the study area trend northeast-southwest, north-northeast-south-southwest, and northwest-southeast, which may serve as migratory pathways or traps for hydrocarbon accumulation. Additionally, the SPI and the 2D magnetic depth models reveal that the thickness of the sedimentary beds ranges from over 1000 m to over 5000 m. Depths between 3000 m and 5000 m can be found in the central, eastern, southeastern, and northeastern parts of the study area. These areas correspond to Alkaleri, Akko, Gombe, Futuk, Yuli, and Debar Fulani, respectively. The depth range of 3000 m to 5000 m is sufficient for hydrocarbon maturation and accumulation. The positive DRAD values indicate zones of probable hydrocarbon potential. The estimated total RHP rates for the study area range from 289.4 to 1477.6 ρwkg^{-1}. The RHP values exceeding 797.87 Wkg^{-1} obtained in the Keri-Keri Formation (Kst) and Pindiga Formation (Psh are attributable to clay, limestone, shale, and sandstone. This falls within the moderate RHP range (750–1500 ρWkg^{-1}), which is adequate for hydrocarbon maturation and accumulation in the study area.

Keywords: Gamma-ray spectrometry, hydrocarbon prospecting, radiogenic heat production, thorium normalisation techniques, subsurface crustal

*Corresponding author: taiwo.adewumi@science.fulafia.edu.ng

1 Introduction

Among the many techniques used to explore hydrocarbon resources are geophysical techniques, which have proven useful and effective in targeting productive basins as well as delineating lithological units, geological boundaries, structures, and heat flux within these basins during both the early and post stages of exploration (Wang et al., 2019). The integration of these techniques effectively determines the nature of the subsurface crust and structures, providing an estimate of the thermal model of the Earth's crust for petroleum and mineral exploration (Elkahateeb and Abdellatif, 2018; Adewumi et al., 2021a; Adewumi et al., 2023).

Hydrocarbon exploration in the Earth's crust can be enhanced through combined geophysical approaches such as magnetic and gamma-ray spectrometric (GRS) methods. The magnetic method has proven useful for identifying subsurface geological structures that may serve as migratory paths or traps for hydrocarbons, as well as for assessing crustal thickness and the thickness of sedimentary cover relevant to hydrocarbon maturation and accumulation in a sedimentary basin (Araffa et al., 2018; Adewumi et al., 2023). The characteristic signatures of these methods in oil and gas deposits reveal various lithological and structural factors that are crucial in hydrocarbon exploration. Furthermore, the GRS has been employed in lithological differentiation (Ademila et al., 2018; El Qassas et al., 2020), determining geochemical characteristics (He et al., 2016), radiogenic heat production (RHP) (Ehinola et al., 2005; Ali and Orazulike, 2010; Oyebanjo et al., 2020; Akingboye et al., 2021, 2022; Adewumi et al., 2023), and evaluating the hydrocarbon potential of the Earth's crustal formations (Saunders et al., 1993; Al-Alfy et al. 2013; Walker et al. 2018; Adewumi et al., 2021b). In this study, these methods will provide a detailed account and understanding of the subsurface geological architecture controlling the hydrocarbon potential in the study area.

This study, therefore, employs the airborne magnetic and GRS datasets of the Gongola basin in the Upper Benue Trough (UBT) to map the shallow-to-deep structural elements and thermal structures using analytic techniques such as vertical derivatives, total horizontal derivative, Rose diagram, source parameter imaging, 2D magnetic depth modelling, thorium normalisation method, and RHP, which will contribute to the lithostructural and depth characterisation and the thermal model for hydrocarbon exploration in the study area.

2 Geological Settings and Location of the Study Area

The study area (Gongola basin), which is one of the inland basins in Nigeria, falls within the Upper Benue trough bounded by Longitude 10.0^{o} – 11.0^{o}E and latitude 9.50^{o}- 10.50^{o}N with an estimated total area of 12,100 sq.km (Fig. 1). The Gongola basin (GB) is one of the arms of the Upper Benue trough. It is an N-S trending arm of the 1000 km long Benue Trough, which contains 5 km thick sediment accumulations (mainly Cretaceous) deposited under mutable environments (Epuh and Joshua, 2017). The sediments have undergone several tectonic phases, which account for the observed folding, faulting, and fracturing of the rocks. The GB is an adjoining basin linking the Benue Trough with the Bornu (Chad) Basin, forming part of the West African Rift System (WARS).

Stratigraphically, the GB comprises

the following formations: The Alluvium deposition, Yolde Formation (Yls), Pindiga Formation (Psh), Gombe Formation (Gst), and Keri-Keri Formation (Kst), alongside crystalline rocks such as Granite Gneiss (GG), Porphyritic granite (oGp), Charnockitic (Ch), Migmatite (m), and Fine-grained granite (oGf) (Fig. 2). The Pindiga Formation consists of marine shales with limestones near the base, which are fossiliferous and have yielded a lower Turonian fauna age. The contact between the Fika Shale and the overlying Gombe Formation is not well exposed but may be unconformable, justifying the placement of the Fika Shale in the Pre-Santonian. The Gombe Formation is believed to rest unconformably on older strata dated to the late Senonian. The Keri-Keri Formation lies unconformably on the folded Cretaceous sedimentations of Palaeocene (Tertiary) age (Amiewalan and Bamigboye, 2019)

.

3 Methodology

3.1 Airborne Geophysical Datasets

The airborne geophysical datasets used in this study (magnetic and gamma-ray spectrometry) were procured from the Nigerian Geological Survey Agency (NGSA). The geophysical surveys were carried out between the years 2005 and 2009 by Fugro Airborne Survey on behalf of the Nigerian Geological Survey Agency (NGSA, 2017). The aeromagnetic datasets were collected using a 3X Scintrex CS3 Caesium Vapour Magnetometer. On the other hand, the aeroradiometric datasets were collected using GR-820-3 with radiometric crystal GPX 1024/256. These airborne geophysical data were collected at an interval of 0.1 sec at an altitude of 100 m along a flight line spacing of 500 m in NW-SE, a sensor mean terrain clearance of 80 m, and a tie line spacing of 2 km, with a flight line trend of 125 degrees. For a half-degree sheet, the maps were created on a scale of 1:100,000. The geomagnetic gradient was removed from the aeromagnetic data using the International Geomagnetic Reference Field (IGRF) of the

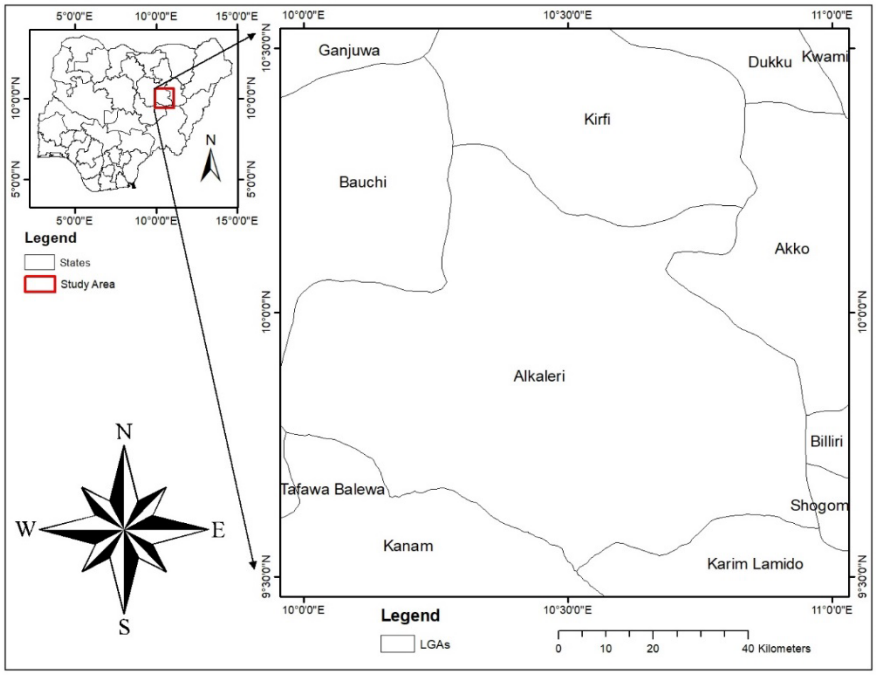

Figure1. Location map of the study area.

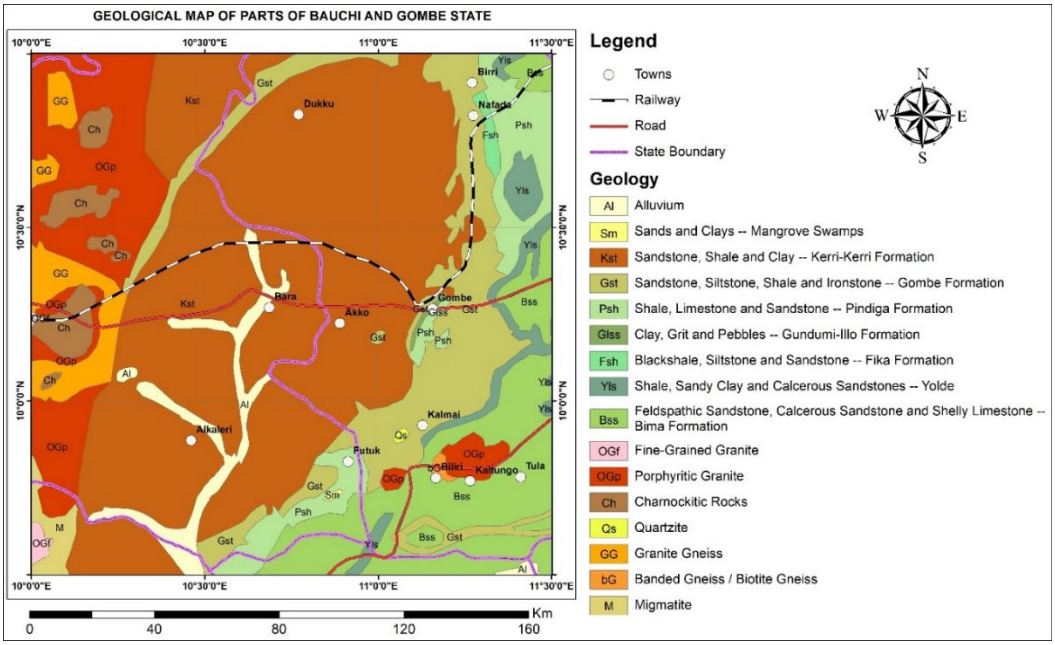

Figure 2. Geological map of the study area.

January 2005 model and referenced to the 1984 World Geodetic System (WGS) ellipsoid. The acquisition agency also processed the GRS datasets to correct background radiation arising from cosmic rays and aircraft anomalies due to altitude changes relative to the ground. The corrected data provided the exact measured elemental concentrations of K, eU, and eTh.

The study area is made up of four (4) half-degree by half-degree (55 by 55 sq. km) data sheets of airborne magnetic and radiometric datasets which were knitted and used to produce the composite map of the total magnetic field (TMI) and the radioelement concentration maps (K, eTh, and eU) of the study area, respectively. All the datasets used for this study were filtered, enhanced, and processed using the Oasis Montaj^{TM} software. The TMI gridded data were reduced to the magnetic equator to ensure proper placement of the magnetic anomalies over their causative bodies. Hence, the TMI reduced to the equator (RTE-TMI) data were further analysed to produce the vertical derivative maps, rose diagram, source parameter imaging (SPI), and 2D magnetic depth modelling. Likewise, the K, eTh, and eU were also used to produce the radiogenic heat production (RHP) maps and delineation of radioactive anomalies derivative map (DRAD) from thorium normalisation techniques (TNT). All the analysed maps were used to delineate the shallow-deep structural elements and thermal structures responsible for hydrocarbon maturation and accumulation within the study area.

3.2 Litho-structural classification

3.2.1 First and Second Vertical Derivatives (FVD and SVD)

Vertical derivatives (VD) filtering is are effective tool useful for litho-structural mapping, such as mapping intra-sedimentary volcanic rocks and geological structures, lineaments, trends, geological contacts, and edge magnetic source bodies (Anudu *et al*. 2014). VD generally highlights the borders of anomalies and

improves the physical representation of shallow causative geological formations. VD also narrows anomaly widths and precisely recognises or detects geological body contacts/boundaries. Hence, it is used in this study to delineate geological structures that might serve as migratory paths/traps for hydrocarbon accumulation within the study area. The first- and second-order vertical derivatives are defined as follows (Anudu *et al*. 2014):

$$FVD = -(\partial T/\partial Z) \quad (1)$$

$$SVD = (\partial^2 T/\partial Z^2) \quad (2)$$

where FVD is the first vertical derivative, SVD is the second vertical derivative, and T is the total magnetic field.

3.3 Thorium Normalisation Techniques (TNT)

The TNT employs equivalent thorium (eTh) parameters as a lithological control to get the eU and K ideal values (Elsadek, 2022). This technique was established by Saunders et al. (1987) and was first used for the delineation of hydrothermal regions in Grixias-Guarinos. Afterwards, several authors such as Adewumi et al. (2021), Ghoneim et al. (2021), and Mamouch et al. (2022) have also employed this technique for hydrocarbon and mineral prospecting. The concept of this technique arises from the fact that lithology and environment contribute to the concentration and distribution of the naturally occurring radioelements (K, eTh, and eU) on the Earth's surface (Saunders et al., 1987 and Pires, 1995). As a result, it is stated that data normalisation for eTh would suppress the original effects of all undesired variables. Thorium (eTh) is used as a normaliser because of its lower geochemical mobility compared to K and eU (Adams and Gasparini, 1970). The TNT is based on the following relation:

$$K_i = \left(\frac{meanK_s}{meaneTh_s}\right) * eTh_s \quad (3)$$

$$U_i = \left(\frac{mean\ U_s}{mean\ eTh_s}\right) * eTh_s \quad (4)$$

Where Ki is the estimated equivalent thorium-defined potassium value for the station with a real equivalent thorium value of eThs. And U_i is the calculated equivalent thorium-defined equivalent uranium value for that station. Variations of the real values from the estimated ideal values for each station were obtained using the equation of the form (Saunders et al., 1993):

$$KD\% = \frac{(K_s - K_i)}{K_i} \quad (5)$$

$$eUD\% = \frac{(eU_s - eU_i)}{eU_s} \quad (6)$$

where K_s and eU_s are the measured potassium and equivalent uranium values at the station, respectively. *KD%* and *eUD%* are the relative deviations expressed as a fraction of the station values. From experience, *KD%* yields small negative values and *eUD%* yields smaller negative or sometimes positive values over the hydrocarbon accumulations (Saunders et al. 1993). Emphasising these two relationships, Saunders et al. (1993) defined a new parameter, called delineation of radioactive anomalies (DRAD).

$$DRAD = eUD\% - KD\% \quad (7)$$

Hence, positive *DRAD* values are favourable indicators for subsurface hydrocarbon accumulations in an area (Saunders et al. 1993).

3.4 Estimation of radiogenic heat production (RHP) and hydrocarbon potential

RHP is one of the crucial mechanisms for hydrocarbon generation and accumulation in sedimentary basins (Oyebanjo et al., 2016). The RHP of the Gongola Basin will provide new insights into the

thermal model for hydrocarbon prospecting in the study area. The RHP was estimated for the lithological units of the study to account for the radiogenic heat (Q) generated by each formation for hydrocarbon exploration. The radioelements are found in various concentrations in the Earth's crust, and heat generation varies significantly with lithological units due to variations in the concentration of the radioelements (K, eTh, and eU) (Haack 1982; Cermark and Rybach 1982). The amount of ^{238}U in natural uranium is 99.28 per cent, 235U is roughly 0.71 per cent, and the rest is ^{234}U. Although the radioactive isotope ^{40}K is just 0.01167 per cent abundant in natural potassium, it is a common element with significant heat output. The heat created per second by these elements (in Wkg^{-1}) is 95.2 for eU, 25.6 for eTh, and 0.00348 for K. (Haenel et al., 1988). Eq. 8 was used to calculate the Q in rocks with eU, eTh, and K concentrations. As a result, the sum of the individual heat produced by eU, eTh, and K was used to compute the overall radioactive heat contribution from the research region.

$$Q(\rho Wkg^{-1}) = 95.2C_u + 25.6C_{Th} + 0.00348C_K \quad (8)$$

Where Q is the RHP, while C_U, C_{Th}, and C_K are the elemental concentrations of eU, eTh, and K, respectively.

Also, the RHP of representative lithology across the study area was derived from maps to infer the RHP for assessing the hydrocarbon potential of each formation. The radioelement maps were sampled to obtain the concentration values across the study area. This was carried out by drawing profiles across the three radioactive elements grids for the geological units in the study area. All the formations were considered during sampling to know the amount of heat flow generated from the source rocks within the study area for petroleum generation.

4 Results

4.1 Total magnetic intensity (TMI), Residual and TMI- Reduce to Equator (RTE) Maps

The total magnetic intensity (TMI) map (Fig. 3a) was generated to showcase the distribution of magnetic sources within the area of study. High magnetic responses (HMRs) are represented in red to pink colours, while moderate (MMRs) to low magnetic responses (LMRs) are depicted in yellow to blue colours, respectively. The positioning of magnetic signatures on the TMI map agrees quite with the rock types situated on the geology map. The HMRs are seen to align with regions occupied by porphyritic granite on the western parts and ironstones on the southeastern edge. The central NW regions, with part of the SW, are occupied by major sedimentary rock types which exhibit little or no magnetic properties. To ensure accurate placement of the anomalies over their causative bodies, the TMI was reduced to the magnetic equator (RTE) (Fig. 3b).

4.2 Concentration anomalous maps of radiogenic elements within the study area

The radioelement concentration maps for potassium (K%), thorium (eTh) and uranium (eU) (Fig. 4a-c) were produced in an aggregate of colours, with pink signifying high concentration, green signifying moderate concentration, and blue signifying low concentration (Fig. 6a-d). The maps K, eTh, and eU can be classified as having high, moderate, or low concentrations (HC, MC, and LC, respectively). The three radioelement maps possess HC on the NW and continue to the SW flank of the study area.

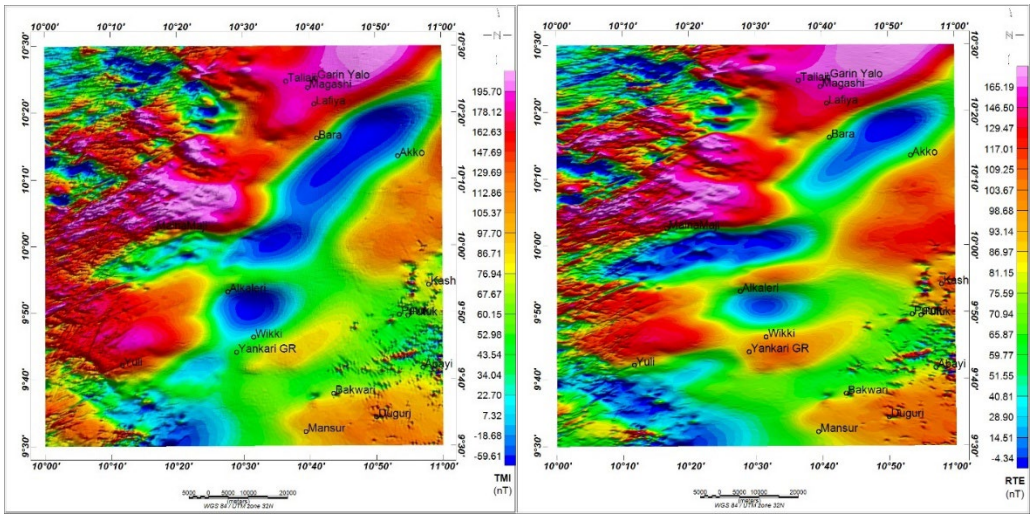

(a) (b)

Figure 3. Magnetic anomalies maps of the study area; (a) TMI, (b) RTE-TMI.

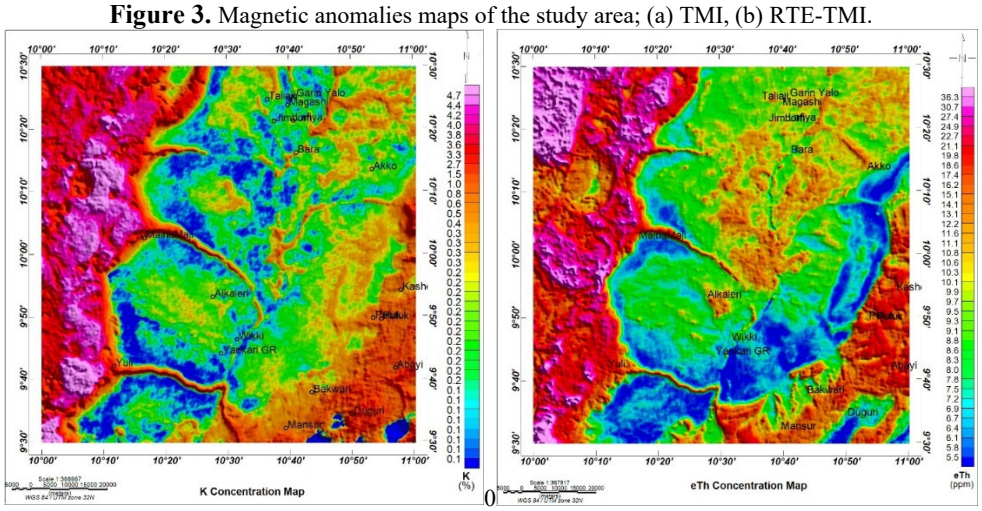

(a) (b)

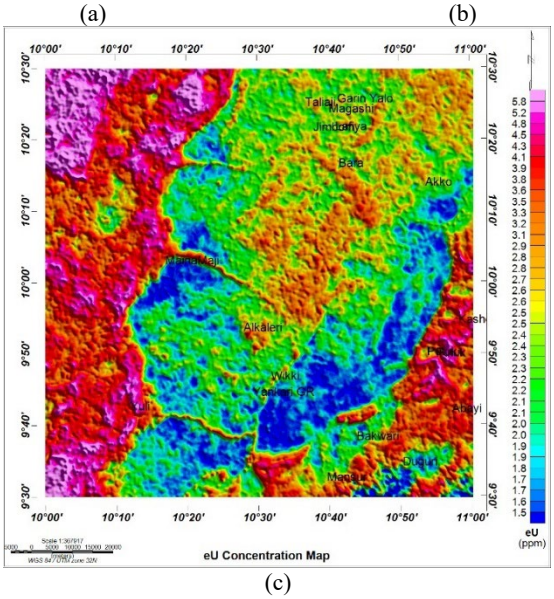

(c)

Figure 4. Radioelement Concentration maps of the study area (a) Potassium (K%), (b) Equivalent Thorium (eTh), (c) Equivalent Uranium Concentration (eU).

MCs are visible on the southeastern part of the study area, while a diagonally oriented LC is observed from the northeast down to the southwest flank of the study area. The HC, MC and LC values of the radioelements range from 1.00 – 4.7 %; 0.2 – 0.6 %; 0.1 – 0.2 % for K, 14.1 – 36.3 ppm; 7.5 – 10.3 ppm; 3.3 – 10.1 ppm for eTh, and 3.2 – 5.8 ppm; 2.1 – 2.8 ppm; 1.5 – 2.0 ppm for eU, respectively. The HC of the three elements concentration at the NW down to the SW part may result from the influence of the shallow depth and outcropping of the crystalline rocks, which corresponds to the porphyritic granite underlying the sediments. Likewise, the HC of K, eTh, and eU in the southeastern part might be attributable to shale (petroleum source rock) in the Yolde Formation. The MC in the northern to central part of the study area corresponds to the Keri-Keri formation, which is composed of sandstone, shale, and clay (Fig. 2). The LC of the three radioelements in the central-southern part is a result of the thick pile of sediments in the Gombe formation.

5 Discussion

The study area (Gongola Basin) is lithologically made up of AL, Kst, Gst, Psh, and crystalline rocks (GG, oGp, Ch, M, and oGf) (Fig. 2). The Kst occupies the north, central, and northwest parts, and accounts for almost 70% of the study area. The Kst is composed of sandstone, shale, and clay. It is dominated by high, moderate, and low magnetic (Fig. 3a-b) and radiometric signatures (Fig. 4a-c). The long-wavelength signatures from the magnetic field might be attributed to thick sedimentary covers. High concentrations of the radioelements (Fig. 4a-c) delineated in the northwestern and southwestern parts of the study area can be attributed to the crystalline rocks. The Gst underlies the KF and overlies the YF in the extreme southwestern part of the study area. The Gst comprises intercalations of siltstones, shale, and ironstones, accountable for the identified low magnetisation and radioelement concentrations. The Psh conformably overlies the Yls in the southeastern part of the study area. It is composed of shales and limestones sandstone; hence, responsible for low to moderate magnetisation and radiometric signatures. The basement intrusion, such as sills and dikes as observed in the northwestern and southwestern parts of the study area, can interact with sedimentary layers to create traps for hydrocarbon in the central to southern portions of the study area. This intrusion can form impermeable seals, preventing the migration of hydrocarbons and trapping them within adjacent porous and permeable sedimentary layers of the study area.

5.1 mapping of shallow-to-deep subsurface structural elements: Insights from magnetic analytical modeling

Subsurface geological structures (faults, lineaments) are vital in hydrocarbon exploration as they help control the migration of oil and gas from the source rocks (Anudu et al., 2014). The FVD (Fig. 5a) and SVD (Fig. 5b) are crucial in hydrocarbon exploration as they explicitly delineate geologic structures responsible for the migration of oil and gas from the source rocks. The occurrences and extent/lateral boundaries of the rock formations within the study area were recognised and mapped. The study area comprises sedimentary sections and a basement complex. The basement complex occupies the northwestern to the southwestern part of the study area. The geological structures delineated in the VD and SVD maps (Figs. 5a-b) are categorised into four major parts: the NE-

SW, NNE-SSW, NW-SE, and E-W, as exposed by the rose diagram (RD) (Fig. 5c). The major structures trend NE-SW and E-W. While the minor structural features, on the other hand, are oriented NW-SE and NNE-SSW. The trends of these geological structures suggest that the area of study might have witnessed several phases of tectonic deformation at different geological times, as explained by Genik (1992) and Okosun (1995). The northwestern, western, and southwestern made up of crystalline rocks, are dominated by NE-SW oriented structures. The sedimentary sections within the study are also composed of NE-SW and E-W oriented structures, which might serve as a migratory or trap for the hydrocarbon accumulation from the source rocks to the reservoir. Remarkably, the structural trending agrees with the dominant NE-SW trending fault system (Aduroju et al., 2016).

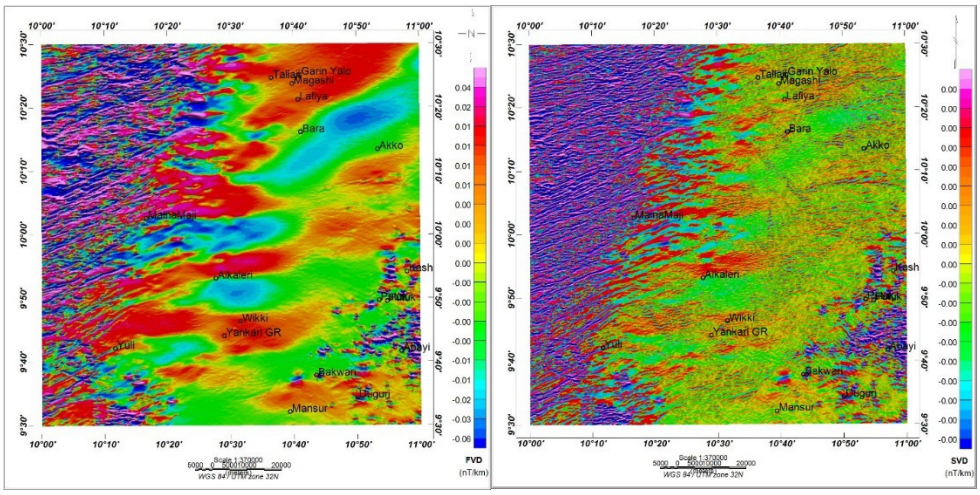

Figure 5. (a) First vertical derivative map, (b) second vertical derivative map, (c) Rose diagram of the study area.

To better understand the shallow-deep structural elemental features, basement architecture, and the sedimentary thickness of the study area for hydrocarbon

exploration, 2D depth magnetic modelling was performed using the RTE-TMI of the study area. The modelling technique is a two-dimensional forward modelling, which is done with the gravity/magnetic system (GM-SYS) extension in Oasis Montaj software version 8.4. The application is an interactive forward modelling program that calculates the gravity/magnetic response of a hypothetical geologic model defined by the user. Along with the RTE-TMI used were other data, such as the Shuttle Radar Topography Mission (SRTM) for topography enhancement and SPI (Fig. 6) for depth control, which reveals a thickness of sediments ranging from 102.0 – 5078 m. The terrain clearance used was 80 m, which was added to obtain the magnetic elevation. In this study, three profiles: A-A', B-B', and C-C', were carefully selected across some significant structures on the RTE-TMI anomaly map (Fig. 3b), in N-S and NE-SW directions from the northern (Kst) through the central (AL) to the southern (Kst) parts, and from the north-eastern (Kst) through the central (Kst) to the southern part (Gst and Psh) of the study area.

Observed on the models (Fig. 7a-c) is the best fit between the calculated and observed magnetic field anomalies with slight errors. In model A-A' (Fig. 7a), a sedimentary thickness of approximately 4.2 km in the Keri-Keri formation (Kst) was recorded at a distance of 18 km in the northern part of the study area. Also, within the Kst, at a distance of 30 km, an uplift of 1.3 km was observed, which is likely an intrusion into the sediments. Towards the central part, a depth of 2.2 km was delineated. In general, the sedimentary thickness obtained from model A-A' ranges from 1.3 – 4.2 km. Likewise, a sedimentary thickness of 4.0 km was observed for model B-B' (Fig. 7b) at a distance of 20 km in the northern part of the Kst. At the central part, a depth to the top of the basement 2.5 was recorded. At the southern part of the Gombe Formation (Gst), a depth of 2.0 was obtained. So generally, the sedimentary thickness obtained from model B-B' ranged from 2.0 – 4.0 km.

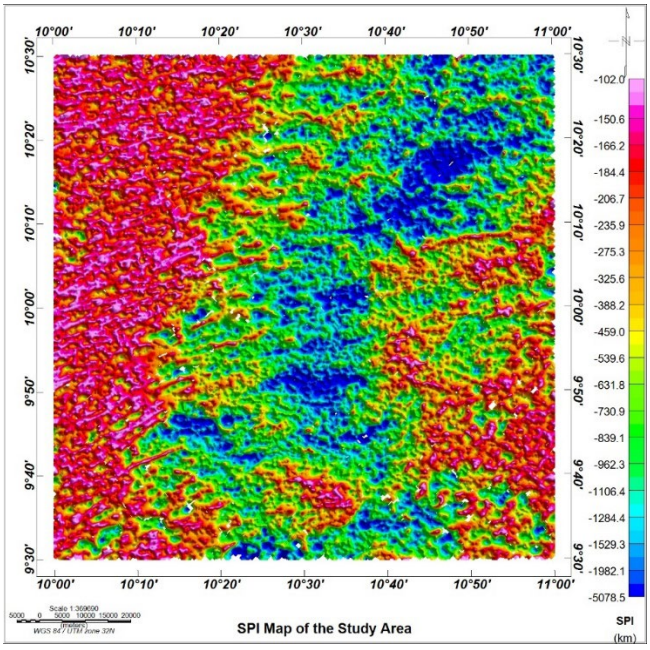

Figure 6. Source parameter imaging map of the study area.

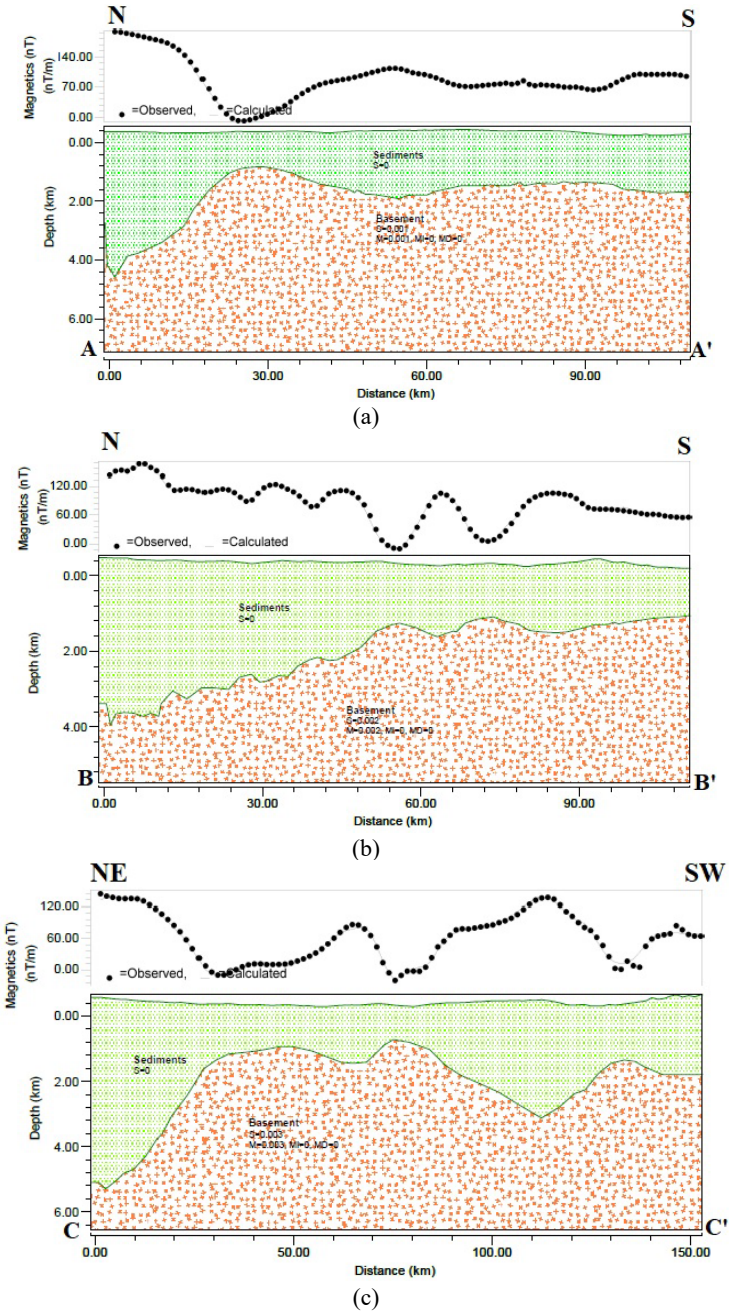

Figure 7. 2D models of profiles; (a) A-A' in N-S, (b) B-B' in N-S, and (c) C-C' in NE-SW directions produced from the RTE-TMI map of the study area.

A thickness of 5.0 km within the Kst was obtained from model C-C' (Fig. 7c). At a distance of 40 km, an uplift of 1.8 km into the sediments was noticed, signifying basement intrusion in the central region. Towards the southwestern part of the Gombe formation (Gst), a sedimentary pile of 3.3 km was obtained, and in the extreme part, a depth of 1.8 km was recorded in the basement complex. A sedimentary thickness of >3.0 km to about 5.0 km was obtained in the northern and central part of the Kst, which is sufficient for hydrocarbon maturation and accumulation within the study area. All the models reveal that the basement

architecture is not flat topographically but undulated, with sediment magnetic susceptibility contrast of 0.0, while the basement had susceptibility and magnetisation in the range of 0.001–0.003 and 0.001–0.003, respectively.

5.2 Possible regions of hydrocarbon exploration within the study area: Insight from thorium normalisation technique (TNT), radiogenic heat production (RHP) and SPI

Figs. 8a-c depict the relative deviations of potassium (KD%), equivalent uranium (eUD%), and delineation of radioactive anomalies (DRAD) maps, which reveal the residual contents of the hydrocarbon anomalies of the study area. These maps (Figs. 8a-c) clearly show anomalies that might be indicative of potential hydrocarbon accumulation zones within the study area. The KD%, eUD%, and DRAD reveal regions of negative and positive anomalous values, which range from -24.7 – 18.9 %, -0.5 – 0.3 %, and -18.9 – 25.7 %, respectively. Observed on Fig. 8a, the northeastern part through the centre to the southern part of the study area is dominated by negative anomaly values with some patches of positive values, which fall within the Keri-Keri Formation (Kst). The northwest, west, and southeastern parts of the study area are also dominated by positive values, which fall within the basement complex. On the other hand, Fig. 8b and Fig. 8c are the opposite expressions of Fig. 7a. Previous studies have shown that hydrocarbon accumulations within sedimentary regions are characterised by negative KD% and positive DRAD (Saunders et al.,1993, Adewumi et al., 2021, etc.). The black circles on the DRAD map are the more positive DRAD anomaly values, which are indicators of favourable regions of hydrocarbon accumulation within the study area. The regions correspond to the areas delineated on the SPI map and the 2D magnetic depth models that are characterised by over 3.0 km of sedimentary thickness.

The calculated RHP from the radioelements (K, eTh, and eU) ranges from 0.00 to 0.02 $\rho W \mathrm{k} g^{-1}$; 141.1 to 930.3 $\rho W \mathrm{k} g^{-1}$; and 142.1 to 553.2 $\rho W \mathrm{k} g^{-1}$, respectively (Figs 9a-d). Their total heat ranges from 289.4 to 1477.6 $\rho W \mathrm{k} g^{-1}$. The calculated RHP for the study area is classified into three major categories: low heat production (LHP), ranging from 0.00 to 0.00 $\rho W \mathrm{k} g^{-1}$; 141.1 to 258.8 $\rho W \mathrm{k} g^{-1}$; and 142.1 to 240.0 $\rho W \mathrm{k} g^{-1}$; moderate heat production (MHP) ranging from 0.00 to 0.01 $\rho W \mathrm{k} g^{-1}$; 264.1 to 539.0 $\rho W \mathrm{k} g^{-1}$; and 245.0 to 344.8 $\rho W \mathrm{k} g^{-1}$; and high heat production (HHP) ranging from 0.01 to 0.02 $\rho W \mathrm{k} g^{-1}$; 581.9 to 930.3 $\rho W \mathrm{k} g^{-1}$– 1; and 358.9 to 553.2 $\rho W \mathrm{k} g^{-1}$, respectively, as observed in (Figs. 9a-d). Likewise, the total RHP can be categorised into LHP ranging from 289.4 to 498.1 $\rho W \mathrm{k} g^{-1}$, MHP ranging from 508.2 to 932.8 $\rho W \mathrm{k} g^{-1}$, and HHP ranging from 988.9 to 1477.6 $\rho W \mathrm{k} g^{-1}$ (Fig. 9d). The RHP maps (Figs. 9a-d) reveal that the northwest, west, and southwest regions of the study area produced more radiogenic heat than the rest of the area, corresponding to Kashere, Abayi, and Maina Maji, which is due to the dominating crystalline rocks (Porphyritic granitic rocks). The LHP observed in the northeastern and southeast parts of the study area, corresponding to Duguri, Yankari GR, and Wikki, can also be attributed to the alluvium deposition. The MHP observed in the central flank, which corresponds to Akko, Alkaleri, Bara, Mansur, Putuk, and Jimbom within the Keri-Keri Formation (Kst),

could be attributed to shale and limestone (petroleum source rock) (Fig. 2). The interpretations align with the previously discussed radionuclide maps in the study area. Therefore, regions with the MHP rate of values >750 $\rho W \mathrm{k} g^{-1}$within the sedimentary section of the study area are significantly viable for hydrocarbon maturation zones (Ehinola et al., 2005; Oyebanjo et al., 2016) and exploitable at depths of 3 km and above, especially in the deep-seated regional faults/fractures within the study area. The obtained RHP of the Gongola Basin has offered new insights into the thermal model for hydrocarbon prospecting in the study area, which is one of the mechanisms in hydrocarbon exploration in a sedimentary terrain. The results also agree with the values of RHP obtained in the Bornu Basin (Adewumi et al., 2023).

Table 1 summarises the statistical results of the three variables (DRAD, RHP, and SPI) across the rock units of the study area, focusing on their potential for hydrocarbon resources. The essential parameters indicating hydrocarbon accumulation in this study (DRAD and RHP) were further subjected to statistical

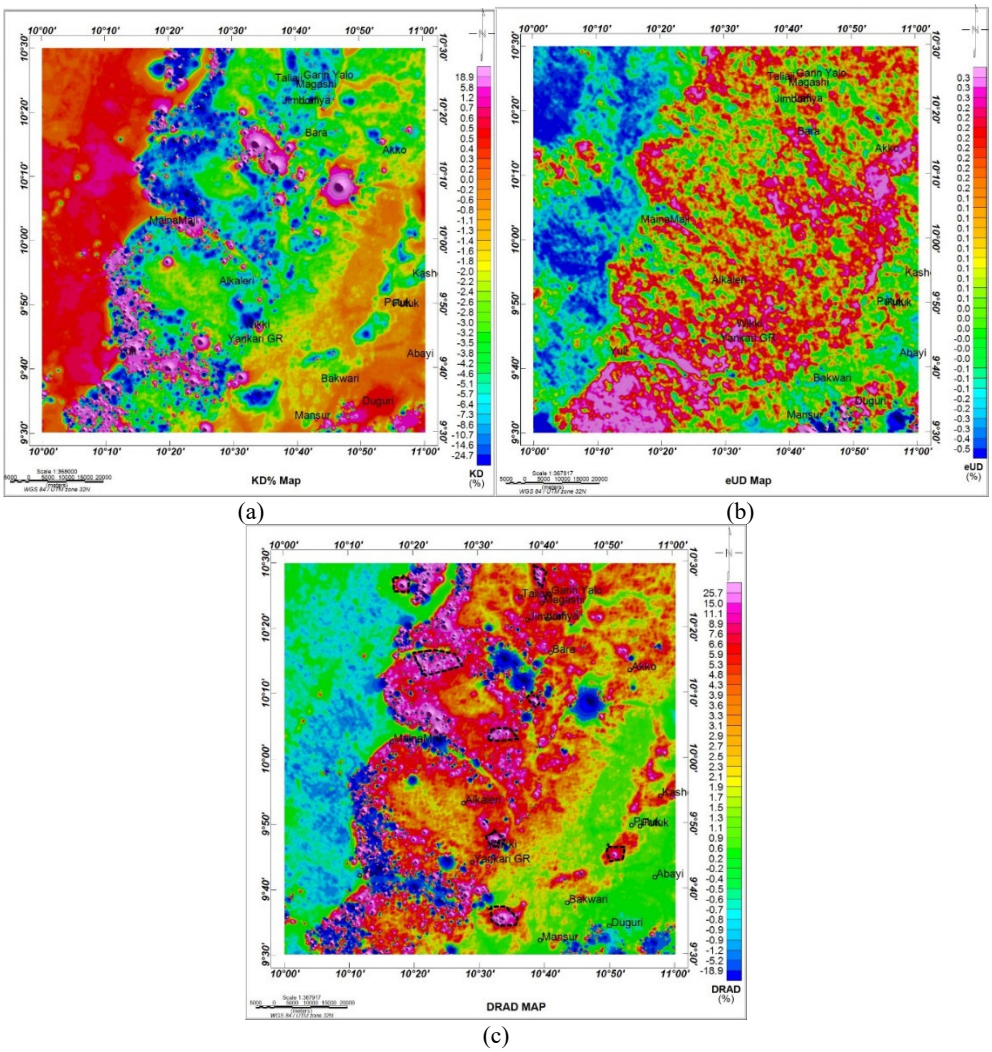

(a) (b)

(c)

Figure 8. (a) KD% anomaly map (b) eUD% anomaly map (c) DRAD anomaly map (black circles refers to the positive DRAD anomalies).

Table 1. Summarized computed DRAD, RHP, and SPI for each rock unit to identify probable hydrocarbon accumulation zones in the study area.

Rock type	Lithologic rock unit	Geological age	Parameters	Min	Max	Mean	SD	CV%	Sedimentary Thickness SPI (m)
Sedimentary	Bss	Cenomanian	DRAD (%)	-226.22	109.17	-1.00	13.42	-1342	3906.00
			RHP (ρW/kg)	347.50	808.75	501.57	131.03	26.12	
	Psh	Cenomanian- Turanian	DRAD (%)	-0.20	2.20	0.86	0.50	58.14	2463.40
			RHP (ρW/kg)	460.5	723.1	574.23	66.6	11.59	
	Al	Quartenary	DRAD (%)	-209.84	479.84	5.72	26.92	470.63	3494.30
			RHP (ρW/kg)	320.98	589.12	435.40	67.66	15.53	
	Gst	Maastrichian	DRAD (%)	0.13	9.40	1.96	1.36	69.39	2699.70
			RHP (ρW/kg)	465.8	823.63	621.33	104.83	16.87	
	Kst	Paleocene	DRAD (%)	-2454.3	3372.37	4.265	159.615	3742.43	4870.50
			RHP (ρW/kg)	306.55	701.275	432.66	84.69	19.57	
Basement Complex	M	Precambrian	DRAD (%)	-383.9	584.56	0.23	61.63	26795.65	1249.10
			RHP (ρW/kg)	755.63	1323.8	990.16	153.53	15.48	
	Ogp	Abian-Turanian	DRAD (%)	-833.4	2529.5	2.00	109.53	5476.50	635.20
			RHP (ρW/kg)	702.53	1256.76	953.10	155.16	16.27	
	Ch	Quartenary	DRAD (%)	-1.7	0.13	-0.73	0.33	-45.21	425.10
			RHP (ρW/kg)	496.46	1025.46	655.83	137.96	21.04	
	Ogf	Precambrian	DRAD (%)	-139.2	1830.66	11.00	139.06	1264.18	721.30
			RHP (ρW/kg)	941.06	1916.33	1424.63	294.06	20.64	
	GG	Precambrian	DRAD (%)	-53.925	87.525	-1.575	7.05	449.04	554.40
			RHP (ρW/kg)	910.05	1749.47	1301.92	236.92	18.19	

Bss – Bima Formation, Gst-Gombe Formation, Psh-Pindiga Formation, Kst-Keri-Keri Formation, Al-Alluvium, GG-Granite Gneiss, OGp-Porphyritic Granite, Ch-Charnockitic Rocks, OGf-Fine-Grained Granite.

evaluations to measure their degree of homogeneity and distribution across lithological formations. A statistical measure called the coefficient of variability (CV%) was applied to achieve this. Analytically, a CV% of less than one hundred per cent indicates positive variability and coherent distribution of the measured parameters over the given lithology. As presented in Table 1, the CV% of

DRAD and RHP was estimated over sedimentary and basement complex lithological formations. The RHP parameter exhibited a well-behaved distribution across all lithological formations, with CV% values ranging from 11.59% to 26.12%. Positive DRAD variability was recorded in the Pindiga and Gombe formations, which comprise Psh (Shale, Limestone, and Sandstone) and Gst (Sandstone, Siltstone, Shale, and Ironstone) lithological units, respectively. Additionally, the sedimentary thickness associated with the lithological formations, estimated via Source Parameter Imaging (SPI), shows a deeper sedimentary thickness of 4870.50 m. The Kerri-Kerri and Bima Formations recorded thicker sediments of 3.0 km and above, along with positive DRAD and moderate RHP, which are sufficient for hydrocarbon maturation.

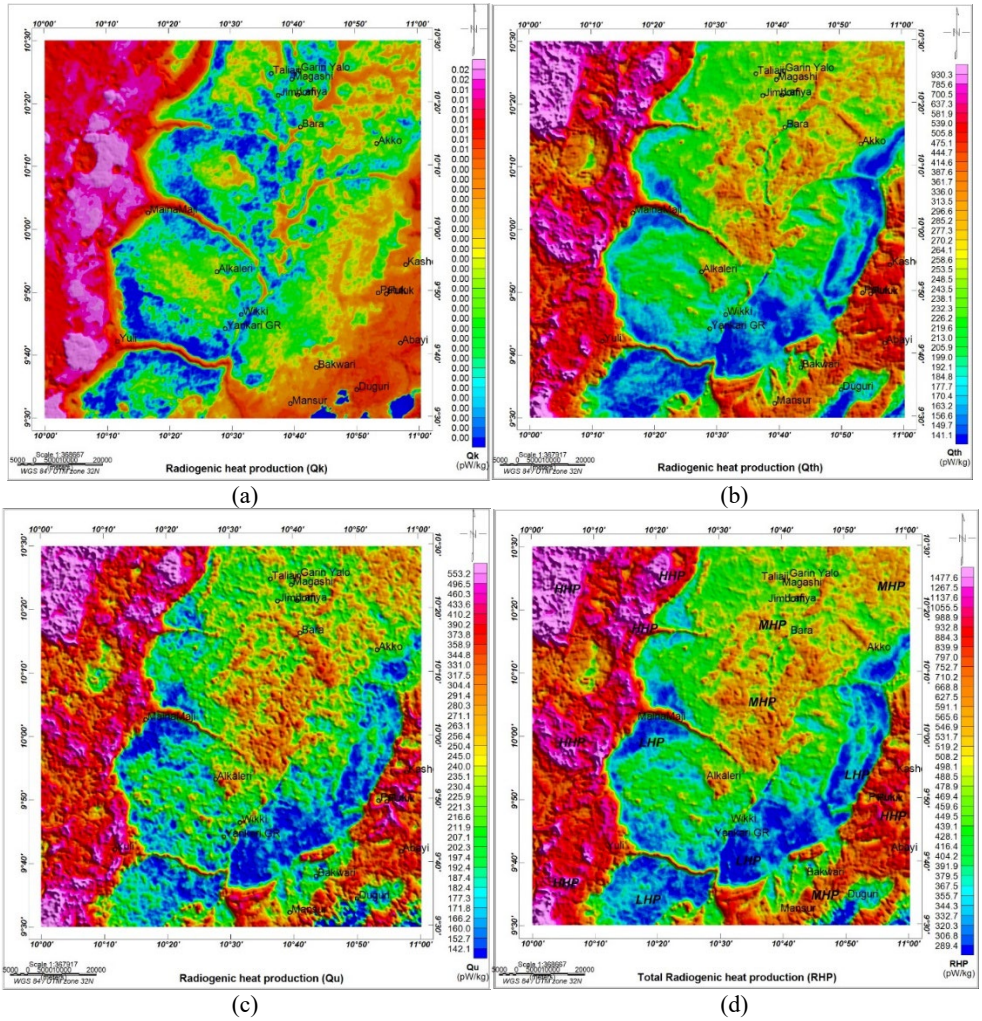

Figure 9. Fig 12: RHP maps of; (a) K concentration, (b) eTh concentration, (c) eU concentration, and (d) heat produced by the three radioelements.

5.3 Integration map of DRAD, RHP, and SPI: hydrocarbon potential indicator in the study area

Fig. 10 is the integrated map of DRAD, RHP, and SPI produced in an aggregate of colours: blue for DRAD, green for RHP, and orange for SPI. These parameters are good indicators of hydrocarbon

potential in sedimentary terrain and have proven useful in delineating regions of hydrocarbon potential on a reconnaissance basis. The map was produced using a cutoff value for each of the maps that are of interest to hydrocarbon prospecting. For DRAD, a minimum value of 5% was used, as we are interested in the positive values of DRAD to indicate regions of hydrocarbon potential in the study area. Likewise, for RHP, a minimum value of 750 $\rho W \mathrm{kg}^{-1}$ and a maximum value of 1500 $\rho W \mathrm{kg}^{-1}$ were adopted, which fall within the moderate range considered sufficient for hydrocarbon maturation and accumulation in the study area. The high RHP observed in the northwestern and southwestern parts of the study area may be attributed to the crystalline basement rocks in the study area. The basement intrusion in the western part of the study area might influence the thermal maturity of source rocks, potentially increasing the generation of hydrocarbon. Furthermore, a minimum cutoff value of 2500 m was considered for the SPI, which reveals the thickness of sediments in the study area; this value is regarded as sufficient for hydrocarbon maturation and accumulation in a rift basin (Isyaku et al., 2016; Epuh and Joshua, 2020). The essence of this map is to show the points of intersection for the three parameters. A close examination of the map reveals that the point of intersection for DRAD and SPI lies in the northeastern part, and central to the southern part of the study area, indicating a promising area for hydrocarbon prospecting. Additionally, the point of intersection of the three parameters, indicated by red colour on the map, can be found in the southwestern part of the study area, which falls in the Keri-Keri Formation. This agreement between these parameters serves as a strong indicator for hydrocarbon exploration in the study area.

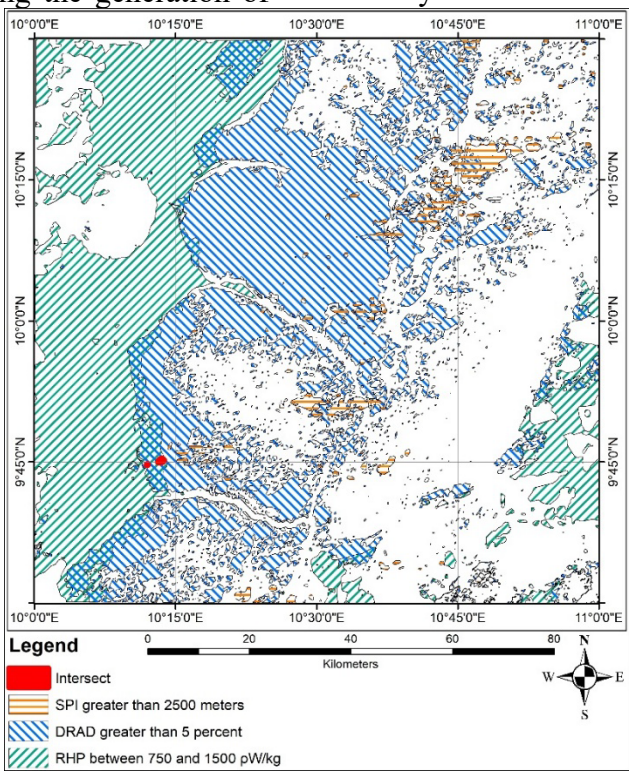

Figure10. Integrated map of DRAD, RHP, and SPI showing the point of intersection of hydrocarbon potential in the study area.

6 Conclusion

This study successfully conducted the mapping of shallow-to-deep subsurface structural elements to determine the thermal regions and hydrocarbon potential of the Gongola Basin from combined airborne magnetic and gamma-ray spectrometric datasets. The results revealed varying lithological and structural features (faults and lineaments) from shallow to deep and the trending of these structures. These distinctive geological features display varying magnetic signatures and radionuclide concentrations. The high magnetic response observed in the northwestern and southeastern parts of the study area may be associated with the influence of the crystalline rock dominating the region. The low to moderate response in the northeastern part, extending through the central to southern parts, may also be linked to thick sedimentary piles. The FVD, SVD, and Rose diagram of the airborne magnetic anomaly maps indicated major lineaments/faults oriented in the NE-SW, NNE-SSW, and E-W directions. These delineated structures might serve as migratory paths or traps for hydrocarbons generated by the hydrocarbon host rocks (shale and limestone) in the study area. The radioelement maps illustrated the variability in the relative abundance of one element compared to another. The SPI map and the 2D magnetic depth models showed the sediment thickness exceeding 3.0 km within the Keri-Keri Formation (Kst), which is adequate for hydrocarbon maturation and accumulation within the study area.

The positive DRAD values indicated zones of probable hydrocarbon potentials. The estimated total RHP rates for the study area range from 289.4 –1477.6 $\rho W kg^{-1}$. The RHP > 797.87 ρWkg^{-1} obtained in the Keri-Keri Formation (Kst) and Pindiga Formation, which are attributable to clay, limestone, shale, and sandstone, falls within the moderate RHP windows (750–1500 ρWkg^{-1}), which is sufficient for hydrocarbon maturation and accumulation in the study area.

References

Adams, J. A., and Gasparini, P. (1970). *Gamma-ray spectrometry of rocks*. Elsevier publishing company.

Ademila, O., Akingboye, A.S., Ojamomi, A.I., (2018). Radiometric survey in geological mapping of basement complex area of parts of Southwestern Nigeria. Vietnam Journal of Earth Sciences 40, 288-298.

Aderoju, A. B., Ojo, S. B., Adepelumi, A. A., & Edino, F. (2016). A reassessment of hydrocarbon prospectivity of the Chad Basin, Nigeria, using magnetic hydrocarbon indicators from high resolution aeromagnetic imaging. *Ife Journal of Science*, *18*(2), 503-520.

Adewumi**, T**., Salako, K. A., Akingboye, A. S., Muztaza, N. M., Alhassan, U. D., & Udensi, E. E. (2023). Reconstruction of the subsurface crustal and radiogenic heat models of the Bornu Basin, Nigeria, from multi-geophysical datasets: Implications for hydrocarbon prospecting. *Advances in Space Research*, (71) 4072–4090. https://doi.org/10.1016/j.asr.2023.01.007.

Adewumi, T., Salako, K. A., Usman, A. D., & Udensi, E. E. (2021). Heat flow analyses over Bornu Basin and its environs, Northeast Nigeria, using airborne magnetic and radiometric data: implication for geothermal energy prospecting. *Arabian Journal of Geosciences*, *14*, 1-19.

Adewumi, T., Salako, K. A., Alhassan, U. D., Adetona, A. A., Rafiu, A. A., & Udensi, E. E. (2021b). Interpretation of Airborne Radiometric data for possible hydrocarbon presence over Bornu basin and its environs, Northeast Nigeria using Thorium normalisation method. *Iranian Journal of Earth Sciences*, *13*(3), 161-172.

Akingboye, A. S., Ademila, O., Okpoli, C. C., Oyeshomo, A. V., Ijaleye, R. O., Faruwa, A. R., Adeola, A. O., & Bery, A. A. (2022). Radiogeochemistry, uranium migration, and radiogenic heat of the granite gneisses in parts of the southwestern Basement Complex of Nigeria. *Journal of African Earth Sciences,* 188, 104469.

Akingboye, A. S., Ogunyele, A. C., Jimoh, A. T., Adaramoye, O. B., Adeola, A. O., & Ajayi, T. (2021). Radioactivity, radiogenic heat production and environmental radiation risk of the Basement Complex rocks of Akungba-Akoko, southwestern Nigeria: insights from in situ gamma-ray spectrometry. *Environmental Earth Sciences*, *80*(6), 1-24.

Al-Alfy, I. M., Nabih, M. A., & Eysa, E. A. (2013). Gamma ray spectrometry logs as a hydrocarbon indicator for clastic reservoir rocks in Egypt. *Applied Radiation and Isotopes*, *73*, 90-95.

Ali, S., & Orazulike, D. M. (2010). Well logs-derived radiogenic heat production in the sediments of the Chad Basin, NE Nigeria. *Journal of Applied Sciences*, *10*(10), 786-800.

Amiewalan, F. O., & Bamigboye, E. O. (2019). Sequence Stratigraphy of Well DX, Gongola Sub-Basin, Upper Benue Trough, Nigeria. *Journal of Applied Sciences and Environmental Management*, *23*(10), 1855-1860.

Anudu, G.K, Stephenson, R.A, Macdonald, D.I (2014). Using high-resolution aeromagnetic data to recognise and map intra-sedimentary volcanic rocks and geological structures across the Cretaceous middle Benue Trough, Nigeria. Journal of African Earth Sciences. 1;99:625-36.

Araffa, S. A. S., El-bohoty, M., Abou Heleika, M., Mekkawi, M., Ismail, E., Khalil, A., & Abd EL-Razek, E. M. (2018). Implementation of magnetic and gravity methods to delineate the subsurface structural features of the basement complex in central Sinai area, Egypt. *NRIAG Journal of Astronomy and Geophysics*, 7(1), 162-174.

Čermák, V., & Rybach, L. (1982). Thermal conductivity and specific heat of minerals and rocks. *Landolt-Börnstein: Numerical Data and Functional Relationships in Science and Technology, New Series, Group V (Geophysics and Space Research), Volume Ia,(Physical Properties of Rocks), edited by G. Angenheister, Springer, Berlin-Heidelberg*, 305-343.

Ehinola, O. A., Joshua, E. O., Opeloye, S. A., & Ademola, J. A. (2005). Radiogenic heat production in the Cretaceous sediments of Yola Arm of Nigerian Benue Trough: Implications for thermal history and hydrocarbon generation. *AGU Fall Meeting Abstracts*, pp. MR11A-0920).

El Qassas, R. A., Salaheldin, M., Assran, S. A., Abdel Fattah, T., & Rashed, M. A. (2020). Airborne gamma-ray spectrometric data interpretation on Wadi Queih and Wadi Safaga area, Central Eastern Desert, Egypt. *NRIAG Journal of Astronomy and Geophysics*, *9*(1), 155-167.

Elkhateeb, S. O., & Abdellatif, M. A. G.

(2018). Delineation potential gold mineralization zones in a part of Central Eastern Desert, Egypt using Airborne Magnetic and Radiometric data. *NRIAG Journal of Astronomy and Geophysics*, *7*(2), 361-376.

Epuh, E. E., & Joshua, E. O. (2017). Gongola Basin Crust-Mantle Structural Analysis for Hydrocarbon Investigation Using Isostatic Residual Gravity Anomalies. *Nigerian Journal of Basic and Applied Sciences*, *25*(2), 51-65.

Epuh, E. E., & Joshua, E. O. (2020). Modeling of porosity and permeability for hydrocarbon Exploration: A case study of Gongola arm of the Upper Benue Trough. *Journal of African Earth Sciences*, *162*, 103646.

Genik, G. J. (1992). Regional framework, structural and petroleum aspects of rift basins in Niger, Chad, and the Central African Republic (CAR). *Tectonophysics*, *213*(1-2), 169-185.

Ghoneim, S. M., Abd El Nabi, S. H., Yehia, M. A., & Salem, S. M. (2021). Using air-borne gamma ray spectrometry and remote sensing data for detecting alteration zones around Wadi Saqia area, Central Eastern Desert, Egypt. *Journal of African Earth Sciences*, *178*, 104181.

Haack, U. (1982). Radioactivity of rocks. In: Hellwege, K. (Ed.), Landolt-Bo¨rnstein Numerical Data and Functional Relationships in Science and Technology. New Series, Group V. Geophysics and Space Research, vol. 1, Physical properties of rocks, subvolume B. Springer-Verlag, Berlin, Heidelberg, New York, pp. 433–481.

Haenel, R., Rybach, L., & Stegena, L. (1988). Fundamentals of geothermics. In: *Handbook of Terrestrial Heat-Flow Density Determination* (pp. 9-57). Springer, Dordrecht.

He, C., Ji, L., Wu, Y., Su, A., & Zhang, M. (2016). Characteristics of hydrothermal sedimentation process in the Yanchang Formation, south Ordos Basin, China: Evidence from element geochemistry. *Sedimentary Geology*, *345*, 33-41.

Isyaku, A. A., Rust, D., Teeuw, R., & Whitworth, M. (2016). Integrated well log and 2-D seismic data interpretation to image the subsurface stratigraphy and structure in north-eastern Bornu (Chad) basin. *Journal of African Earth Sciences*, *121*, 1-15.

Mamouch, Y., Attou, A., Miftah, A., Ouchchen, M., Dadi, B., Achkouch, L.,& Muzirafuti, A. (2022). Mapping of Hydrothermal Alteration Zones in the Kelâat M'Gouna Region Using Airborne Gamma-Ray Spectrometry and Remote Sensing Data: Mining Implications (Eastern Anti-Atlas, Morocco). *Applied Sciences*, *12*(3), 957.

Okosun, E. A (1995). Review of Geology of Bornu Basin. *Journal of Mining and Geology*, 31(2), 113 – 172.

Oyebanjo, O. M., Ajayi, T. R., & Tchokossa, P. (2016). Radioactivity and hydrocarbon generation potential of sediments, Gongola Basin, Nigeria. *Petroleum Exploration and Development*, 43(3), 451-456.

Pires, A. C. B. (1995). Identificação geofísica de áreas de alteração hidrotermal, Crixás-Guarinos, Goiás. *Brazilian Journal of Geology*, *25*(1), 61-68.

Saunders DF, Burson KR, Branch JF, Thompson CK (1993) Relation of thorium-normalized surface and aerial radiometric data to subsurface petroleum accumulations. *Geophysics* 58:1417–1427.

Saunders, D. F., Terry, S. A., & Thompson, C. K. (1987). Test of National Uranium Resource Evaluation gamma-ray spectral data in petroleum reconnaissance. *Geophysics*, *52*(11), 1547-1556.

Walker, S., Keyser, H., Durham, D., & Boaz Oil, L. L. C. (2018). Airborne Gamma-ray surveying in Hydrocarbon Exploration. *GeoConvention, Canada*.

Wang, J., Yao, C., Li, Z., Zheng, Y., Shen, X., Zeren, Z., & Liu, W. (2020). 3D inversion of the Sichuan Basin magnetic anomaly in South China and its geological significance. *Earth, Planets and Space*, 72(1), 1-10.

Wang, Y., Hu, S., Wang, Z., Jiang, G., Hu, D., Zhang, K., ... & Zhang, T. (2019). Heat flow, heat production, thermal structure and its tectonic implication of the southern Tan-Lu Fault Zone, East–Central China. *Geothermics*, *82*, 254-266.